The inclusion complex of 4-hydroxynonenal with a polymeric derivative of B-cyclodextrin enhances the antitumoralefficacyof the aldehyde in several tumor cell lines and in a three-dimensional human melanoma model

TITLE: The inclusion complex of 4-hydroxyonenal with a polymeric derivative of beta-cyclodextrin enhances the anti-tumoral efficacy of the aldehyde in several tumor cell lines and in a three-dimensional human melanoma model.

Stefania Pizzimenti[a,*], Eric Ciamporcero[a], Piergiorgio Pettazzoni[a, 1], Simona Osella-Abate[b], Mauro Novelli[b], Cristina Toaldo[a], Miriam Husse[a], Martina Daga[a], Rosalba Minelli[c], Agnese Bisazza[c], Paolo Ferruti[d], Elisabetta Ranucci[d], Maria Grazia Bernengo[b], Chiara Dianzani[c], Fiorella Biasi[a], Roberta Cavalli[b], Giuseppina Barrera[a].

[a] Department of Clinical and Biological Sciences, University of Turin, Turin, Italy

[b] Department of Medical Sciences, Section of Dermatology, University of Turin, Turin, Italy

[c] Department of Drug Science and Technology, University of Turin, Turin, Italy

[d] Department of Chemistry, University of Milan, Milano, Italy

*** Corresponding author:**

Stefania Pizzimenti

Department of Clinical and Biological Sciences, Section of General Pathology

University of Turin, Corso Raffaello 30, 10125 Turin, Italy.

E-mail address: stefania.pizzimenti@unito.it

Tel +39-011-6707763

[1] Present address: Piergiorgio Pettazzoni, Department of Cancer Biology, UT MD Anderson Cancer Center, Houston, TX, USA

ABSTRACT

4-Hydroxynonenal (HNE) is the most studied end product of the lipoperoxidation process, by virtue of its relevant biological activity. The anti-proliferative and pro-apoptotic effects of HNE have been widely demonstrated in a great variety of tumour cells types *in vitro*. Thus, it might represent a promising new molecule on strategies in anticancer therapy. However, the extreme reactivity of this aldehyde, as well as its insolubility in water, a limiting factor for drug bioavailability, and its rapid degradation by specific enzymes represent the major obstacles for its possible *in vivo* application. Different strategies can used to overcome these problems. One of the most attractive strategies is the use of nanovehicles, since drug loading into nanosized structures enhances their stability and solubility, thus improving their bioavailability and their anti-tumoral effectiveness. Several natural or synthetic polymers have been used to synthesize nanosized structures and, among them, ɓ-cyclodextrin (ɓ-CD) polymers are playing a very important role in drug formulation by virtue of the ability of ɓ-CD ability to form inclusion compounds with a wide range of solid and liquid molecules by molecular complexation. Moreover, several ɓ-CD derivatives have been designed in order to improve their physicochemical properties and inclusion capacities. Here we report that the inclusion complex of HNE with a derivative of ɓ-CD, the ɓ-CD-poly(4-acryloylmorpholine) conjugate (PACM-ɓCD), enhances the aldehyde stability. Moreover, the inclusion of HNE in PACM-ɓCD potentiates its antitumor effects in several tumor cell lines, and in a more complex system, like a human reconstructed skin carrying melanoma tumor cells.

KEYWORDS

4-Hydroxynonenal (HNE)

Nanotechnology

ɓ-Cyclodextrin-poly(4-acryloylmorpholine) conjugate

Tumor cell lines

Three-dimensional human melanoma model

INTRODUCTION

Among different lipid peroxidation-end products, 4-hydroxynonenal (HNE) is the aldehyde most intensively studied by means of its relevant biological activity [1-3]. At micromolar concentrations, similar to those found in human plasma and tissues [4], HNE inhibits cell proliferation, induces differentiation and/or apoptosis [1-2, 5], inhibits angiogenesis [6] and cell adhesion [7], in many tumor cell lines. HNE elicits its biological activities by modulating the expression of oncogenes [8-10], anti-oncogenes [11], transcription factors [12] or apoptotic genes [13-15]. Moreover, HNE is able to affect the unlimited replicative potential of cancer cells, by inhibiting hTERT expression, and consequently telomerase activity, in leukemic and colon cancer cell lines [16, 17]. In the HL-60 human leukemic cell line, the anti-proliferative effect of HNE is also sustained by the modulation of the expression of ten specific miRNAs [11], a class of conserved non-coding small RNAs, which regulate gene expression by translation repression of coding mRNAs [18].

It is very likely that the majority of effects observed on cellular responses can be mediated by the reaction of HNE with biomolecules, such as protein, peptides and, at higher concentrations, with DNA [4, 19]. Quantitatively, proteins, and, among peptides, the GSH, represent the most important group of HNE-targeted biomolecules [4]. The majority of HNE-protein adducts have been identified as enzymes, carriers, receptors, ion channels, transport proteins, cytoskeletal and heat shock proteins. The biological significance of HNE-protein adducts identified have been reviewed by several authors [2, 19]. The HNE adduction occurs through the 1,4-addition (Michael addition) of the nucleophilic groups in cysteine (Cys), histidine (His) or lysine (Lys) residues of the protein, respectively, onto the electrophilic double bond of HNE. Alternatively, Schiff-bases are formed with $\mathring{U}NH_2$ groups of Lys residues via the C-1 aldehyde group. Michael adducts generally represent >99% of HNE protein modifications while Schiff-base adduct formation is less prevalent even in the presence of excess HNE [4, 20, 21].

While the anti-tumoral action of HNE has been widely demonstrated in several tumor cell types *in vitro*, its effect in *in vivo* models has been demonstrated in a very limited numbers of papers. For example, Zarkovic and collaborators have demonstrated that HNE, applied to the skin lesions of melanoma in rats, caused a regression of murine melanoma cell growth and an increased rat survival [22].

The extreme reactivity of this aldehyde, as well as its insolubility in water, a limiting factor for drug bioavailability, and its rapid degradation by specific enzymes [23-26] represent the major obstacles for its possible clinical use. Nanotechnological approaches can help to overcome these problems. Drug delivery systems represent an alternative strategy to reformulate bioactive agents in cancer chemotherapy. Old or new drugs can be loaded into nanosized structures (particularly in the range from 10 nm to 100 nm), thus reducing toxic side effects and improving their therapeutic index. Indeed, the drug encapsulation in a carrier may result in various advantages like better bioavailability, system stability, high drug loading, controlled release kinetics, long blood circulation time and selective distribution in the organs/tissues with longer half-life [27]. Nano-vehicles used for anticancer drug delivery can be made from a variety of materials, including polymers, liposomes, carbon nanotubes, metals, such as iron oxide and gold, and cyclodextrins (CDs) [28]. The latter have received much attention by virtue of their ability to form non-covalent inclusion complexes with a large variety of guest molecules. CDs are biomaterials consisting of natural cyclic oligosaccharides obtained by enzymatic digestion of starch. They consist of glucopyranose units linked by Ŭ(1-4) bond. In particular, the natural ɓ-cyclodextrin (ɓCD), composed of seven glucopyranose units, has been extensively used, by reason of its ready availability and cavity size suitable for the widest range of drugs [29]. However, βCD has low water solubility (1.85 % w/v at 25 °C) and it is toxic when administered intravenously. Consequently many chemical derivatives have been proposed. Among polymer derivatives, amphiphilic β-CDs have been proposed, due to their extremely low toxicity, excellent biocompatibility, and flexible complexation capacity with poorly soluble molecules [29]. In previous work, it has been

demonstrated that a new derivative of ϐCD, the ϐ-cyclodextrin-poly(4-acryloylmorpholine) conjugate (PACM-ϐCD), can be dispersed in water as well as in several organic solvents such as chloroform and lower alcohols [30]. Moreover, *in vitro* tests showed that it is biocompatible, devoid of hemolytic activity and it is capable of including and solubilizing water poorly soluble drugs [30]. The main aim of the present study is to assess the potential anti-tumoral activity of the inclusion complex of HNE with PACM-ϐCD (HNE/PACM-ϐCD). The effects on cell viability, apoptosis and cellular differentiation by HNE/PACM-ϐCD were tested *in vitro* on several tumor cell lines, as well as in a more complex system of human reconstructed skin carrying melanoma tumor cells.

MATERIALS AND METHODS

Preparation and characterization of inclusion complex of HNE with PACM-ϐCD (HNE/PACM-ϐCD)

HNE (Cayman Europe, Tallin, Estonia) is supplied as solution of 10 mg/ml in ethanol. Firstly this solvent was evaporated through a gentle flow of N_2. A solution of acetic acid (CH_3COOH)/acetone (CH_3COCH_3) (Sigma-Aldrich, Milan, Italy) at 30:70 v/v ratio was added to the dried HNE, in an ice bath and under magnetic stirring. PACM-ϐCD was synthesized as described elsewhere [30]. PACM-ϐCD, as powder, was added in a molar ratio 1:1 (HNE: PACM-ϐCD) to the CH_3COOH/CH_3COCH_3 /HNE solution, in order to form the HNE/ PACM-ϐCD (HNE/ PACM-ϐ) inclusion complex. The complex was then dried under nitrogen (N_2) flow, in an ice bath. The dried complex was stored at -20 °C. Before use, the dried complex was completely dissolved in 3 ml of the physiological Phosphate Buffered Saline solution (PBS, containing 0.01 M phosphate buffer, 0.0027 M potassium chloride and 0.137 M sodium chloride, at pH 7.4; Sigma-Aldrich), after at least 2 hours stirring.

The amount of loaded HNE was determined by the HPLC method as described in the next section, after dilution of HNE/PACM-ϐCD in an acetonitrile (C_2H_3N)/CH_3COOH mixture (Sigma-Aldrich) (96:4 v/v).

The HNE/PACM-ϐCD inclusion complex was characterized by Differential Scanning Calorimeter (DSC), by using a DSC/7 differential scanning calorimeter (Perkin Elmer, CT-USA) equipped with a TAC 7/DX instrument controller. The instrument was calibrated with indium for melting point and heat of fusion. A heating rate of 10 °C/min was employed in the 25ï 300 °C temperature range. Standard aluminium sample pans (Perkin Elmer) were used; an empty pan was used as reference standard. Analyses were carried out under N_2 purge; triple runs were done on each sample.

For cell experiment studies, the HNE/PACM-ϐCD inclusion complex as well as, the empty carrier PACM-ϐCDs, were sterilized by autoclaving at 121 °C at 2 bar for 15 min, a crucial passage for their *in vitro*/*in vivo* use. After autoclaving, the HNE stability on HNE/PACM- ϐCD was determined by HPLC analysis (see below).

HNE quantitative analysis in HNE/PACM-ϐCD

The quantitative determination of HNE was performed by HPLC analysis using a Perkin Elmer instrument (L2 Binary Pump) with a UV-vis detector. The mixture of HNE/PACM-ϐCD with the C_2H_3N/CH_3COOH solution, previously described, was separated by HPLC at the following conditions: RP-18 column (Merck, Darmstadt, Germany), C_2H_3N /water (H_2O) 42:58 (v/v) as mobile phase, 1.0 ml/min flow rate, 223 nm optical density UV detector setting with 0.05 absorbance units for full recorder scale, 20 ε M injected sample volume. Peak identification and quantification was based on reference chromatograms and a calibration curve obtained from standard HNE solutions (1 to 10 mM) in H_2O / C_2H_3N / CH_3COOH. The HPLC chromatography system, equipped with an UV-Vis detector and the analytical software were from Waters S.p.A. (Vimodrone, Milan, Italy).

In vitro release study

The *in vitro* release experiments were performed in PBS buffer at pH 7.4 at 37 °C using the dialysis bag technique. About 10 mg of HNE/PACM-ϐCD were dispersed in 3 ml of PBS buffer at pH 7.4 and then placed in a dialysis bag obtained using a dialysis membrane with cut-off 3500 Da (Spectralpor, Spectrum Lab. Inc., Breda, The Netherlands). The dialysis bag was then placed in 15 ml of PBS solution and incubated at 37 °C under stirring. At fixed times within a period of 2 h, samples were collected and replaced with fresh PBS solution. The concentration of released HNE was determined by HPLC analysis, as described above.

Stability of HNE/PACM-ϐCD complex over time

The stability of HNE loaded in PACM-ϐCD, stored at -20 °C, was determined over time by HPLC analysis, as described above, for a period of 12 months.

Evaluation of HNE-His Michael adducts on BSA by Western Blot

10 ε g of BSA diluted in PBS was incubated with 10 ε M free HNE, 10 ε M HNE/PACM-ϐCD, PACM-ϐCD at 37°C for 45 min. Aliquots were then removed from the solutions and HNE-His Michael adducts were measured via Western Blot, as described in ñ*Lysate preparation and Western Blot analysis*ò section of Materials and Methods. The monoclonal primary antibody anti-HNE-His adduct was a kind *gift* of Prof. Uchida. Ponceau red staining was used to confirm equal protein loading.

Preparation and characterization of 6-coumarin PACM-ϐCD inclusion complex

To obtain a fluorescent formulation 6-coumarin PACM-ϐCD inclusion complex was prepared and characterized by DSC and fluorescent spectroscopy as elsewhere described [31].

Cell Culture and Treatments

Human prostate cancer PC-3, human melanoma A375, human leukemia HL-60 and U937, colon carcinoma HT-29 and murine renal cell carcinoma (RenCa) cell lines were obtained from European Collection of Cell Cultures (ECACC). They were cultured at 37 °C in a humidified atmosphere of 5% CO_2-air. All these cells were grown, in RPMI 1640 medium supplemented with 2 mM glutamine, 1% antibiotics and 10% FCS (Lonza).

The treatments with free HNE were performed after the following steps: after evaporating the solvent through a gentle flow of N_2, the aldehyde was then resuspended in sterile PBS. The concentration was measured by spectrophotometer by recording the absorbance of an aliquot of HNE diluted 1:200 in H_2O at 223 nm (Ů=13,750). Cell cultures were treated with a final concentrations of 1, 5 and 10 ε M of free HNE or HNE/PACM-ϐCD, prepared as previously described. Moreover, all the cell lines were treated with empty inclusion complex PACM-ϐCD (for the preparation see above), at dilutions corresponding to that of HNE-loaded inclusion complex.

Cell proliferation and viability

The 3-(4,5-Dimethylthiazol-2-yl)-2,5-diphenyltetrazolium bromide (MTT) assay is a colorimetric assay used to determine the level of metabolic activity in cells, able to reduce the yellow tetrazolium dye MTT to purple formazan crystals. The amount of formazan produced provides an indication of the mitochondrial integrity and activity which, in turn, may be interpreted as a measure of both cell viability and cell proliferation [32]. Cells were seeded (1.5×10^3 - 5×10^5 cells/well) in 96-well plates, in 200 ε l of serum-supplemented medium and were treated with the compounds 24 h later. At the indicated times, 30 ε l MTT dye solution (5 mg/ml in PBS) was added to each well, and the plate was incubated for 3 h at 37°C. After removal of the medium, 150 ε l of dimethyl sulphoxide (DMSO) (Sigma-Aldrich) was added to each well to dissolve the formazan crystals and the absorbance was red at 540 nm on a ELISA plate reader (Perkin Elmer). Each group was analyzed in quadruplicate samples.

Cell viability was evaluated by trypan blue exclusion test also, which is based on the principle that live cells possess intact cell membranes that exclude certain dyes, such as trypan blue. Briefly, cells were plated (1.5 x 10^2 - 4 x 10^4 cells/wells) in 96-well plates, in 200 εl of serum-supplemented medium and were treated with the compounds 24 h later. At the indicated time, a collection of supernatants and adherent cells, obtained by trypsinization, were incubated in 0.4% trypan blue and pipetted onto a Bürker chamber. Stained dead and non-stained viable cells were counted in a microscope and the percentage of live cells was calculated for each experimental condition. Moreover, the viable cells were determined by counting, in a Bürker chamber, the number of non-stained viable cells after trypan blue addition at the indicated time.

Lysate preparation and Western blot analysis

5x10^5 HL-60, PC3 and A375 cells were collected 24 h after the treatments, and washed once in cold PBS, pH 7.4. Total extracts were prepared by lysis in a buffer containing 20 mM Trisï HCl, pH 7.4, 5 mM EDTA, 150 mM NaCl, 1% v/v Triton X-100, phosphatase (P2850, Sigmaï Aldrich), and protease (Sigmaï Aldrich P8340) inhibitor cocktails, incubating them for 15 min at 4 °C. After high-speed centrifugation (10,000 rpm for 15 min at 4 °C), the supernatants were collected, and the protein concentration was determined in triplicate by using a commercially available kit (Bio-Rad Laboratories, Segrate, Milan, Italy). Western blot analysis was performed using home-made 9.3% SDS polyacrylamide gels (Bio-Rad Laboratories). Proteins (20 εg) were mixed with 20 εl of Laemmli sample buffer (161-0737, Bio-Rad Laboratories) containing 10% 2-mercaptoethanol, boiled for 5 min, and loaded into the gels. The run was performed at the constant voltage of 100 V. The proteins were then transferred onto a nitrocellulose membrane with a semidry transfer apparatus (Biometra, Goettingen, Germany). The membranes were subsequently incubated for 1 h with 5% non fat dry milk dissolved in TBSï Tween 20 for saturation of nonspecific binding sites, and incubated overnight at 4 °C with the primary antibodies against the cleaved poly (ADP-ribose) polymerase (PARP) (AB3620, Merck-Millipore, Darmstadt, Germany), or against anti-ϐ-actin

(A1978, Sigmaï Aldrich). The membranes were washed three times with TBSï Tween 20, and incubated with horseradish peroxidase (HPR)-conjugated secondary antibodies (Bio-Rad Laboratories) for 1 h at room temperature. The detection of the bands was carried out after reaction with chemiluminescence reagents (PerkinElmer NEL105001EA) through film (sc-201697, Santa Cruz Biotechnology, Heidelberg, Germany) autoradiography.

HL-60 cell differentiation

Nitroblue tetrazolium (NBT, Sigma-Aldrich) assay was used as a functional measure of the maturation of HL-60 as described by Collins [33] with some modifications. The reduction of NBT to insoluble blue formazan granules occurs during the stimulus-induced respiratory burst of mature granulocytes and is routinely used as an indicator of the extent of granulocytic differentiation of HL-60 acute promyelocytic leukemia cells. Thus, this method allows the detection of differentiated cells capable of producing Reactive Oxygen Species (ROS) as a result of appropriate stimulus, such as phorbol 12-myristate 13-acetate (PMA, Sigma-Aldrich). Approximately 5 x 10^5 cells were resuspended in 0.5 ml PBS containing NBT (200 nM) and PMA (500 nM), the activating agent, and incubated at 37°C for 30 min. 1 N HCl (Sigma-Aldrich) was added to the samples to stop the reaction. The formazan precipitate was solubilized in DMSO and the mixture was transferred to 96-well plates.

The extent of the reaction was evaluated, at 72 and 96 h, by spectrophotometry reading at 570 nm wavelength, on an ELISA plate reader. Results were normalized with the viable cell number and results are expressed in arbitrary units, placing the value 1 to the untreated control cells

Measurement of HNE disappearance from medium

10 ε M HNE/PACM-ϐCD or 10 ε M free HNE were added to 0.5 ml of RPMI medium with 10% fetal calf serum (FCS) (Lonza, Milan, Italy) and maintained at 37 °C in a humidified atmosphere of

5% CO_2. After 0, 5, 15, 30 min, aliquots of medium were added to an equal volume of C_2H_3N / CH_3COOH 96:4 (v/v). HNE content was determined by HPLC analysis, as described above.

Measurement of HNE disappearance from HL-60 cell suspension

HL-60 cells ($5x10^5$) were incubated with 10 εM HNE/PACM-ϐCD or 10 εM free HNE in RPMI medium with 10% FCS (Lonza) and maintained at 37 °C in a humidified atmosphere of 5% CO_2. After 0, 5, 15, 30 min, aliquots of the homogeneus cellular suspensions, were collected for HPLC analysis, as described above.

Evaluation of PACM-ϐCD cellular uptake by confocal laser scanning microscopy in HL-60, PC3 and A375 cells

Exponentially growing HL-60, PC3 and A375 cells were incubated with 1 εg/ml of fluorescent labeled 6-coumarin PACM-ϐCD inclusion complex for 1, 5 and 45 min. The living cells were suddenly observed with a LSM 510 confocal laser microscope (Carl Zeiss SpA, Arese, Milan, Italy), using a plan neofluar lens 20×/0.5 and 40x/0.75 (zoom 2X). The instrument was set to 488 nm exciting laser band, with a 505ï 530 nm band pass emission filter. Exciting light intensity, black level, and photomultiplier gain were adjusted on control specimens; settings were kept the same when scanning experimental samples. Images were elaborated using LSM 510 Image Examiner software (Carl Zeiss SpA). The assay was performed on not fixed living cells, to avoid possible artefacts due to the protocols of cell fixation.

Detection of HNE-His adducts by immunofluorescence in HL-60 cells

HL-60 cells ($5x10^4$) were incubated with 10 εM of free HNE or HNE/PACM-ϐCD. After tretatments, cells were collected at the indicated time, centrifuged and the pellets were fixed for 15 min in 4% paraformaldehyde. Aliquots were smeared onto a non-charged slide and dried. Thereafter the cells were permeabilized with 1% Triton X-100 for 30 min at room temperature and

washed with PBS. Then, the slides were incubated with 1% BSA in PBS for 30 min at room temperature, after which they were incubated for 1 h at room temperature with the primary monoclonal antibody against HNE-His adducts (a generous gift form Prof. Uchida, 1:100 in 1% BSA dissolved in PBS). The slides were subsequently washed, incubated for 1 h at room temperature with the secondary fluorescein isothiocyanate (FITC)-conjugated antibody (Invitrogen, AlexaFluor488 Goat anti mouse IgG, diluted 1:100 in 0.1%BSA in PBS), washed again and mounted on coverslips. The images were captured using an epi-illuminated fluorescence microscope (Axiovert 35; Carl Zeiss MicroImaging GmbH, Jena, Germany), using a plan neofluar lens 40x/0.75.

Melanoma 3D cultures

Culture inserts of a differentiated, full-thickness, three-dimensional skin reconstruction model of A375 melanoma cells were purchased from MatTek (Ashland, MA). These culture inserts were prepared by culturing mixed suspensions of normal human epidermal keratinocytes and A375 melanoma cells at a 1:10 ratio on fibroblast-contracted collagen gels and allowing differentiation for ~1 week. The 3-D tissues are fed only through the basolateral (bottom) surface, where there is the dermal compartment, which remains in contact with the culture medium, while the apical (top) surface of the tissues, corresponding to the cornified epidermal layer, is directly in contact with the air. Culture inserts were then incubated in duplicate with serum-free medium containing 10 ε M HNE/PACM-ϐCD, 10 ε M free HNE and the empty inclusion complex PACM-ϐCD, at the dilution corresponding to that of HNE-loaded inclusion complex, or PBS for control. The medium was replenished every other day, and cell cultures were collected on days 0, 3 and 8 from the beginning of the treatments and fixed with 10% formalin.

For cell morphology analysis, culture inserts were paraffin embedded, serial sectioned, and analyzed by haematoxylin and eosin (H&E) staining. Serial sections were observed under a 10x/1.30 NA objective lens using Olympus BX51 microscope. Images were captured using high-

resolution Leica DFC 420 camera, digitally acquired and edited using Adobe Photoshop CS3 (Adobe Systems Incorporated).

For immunohistochemistry, sections were deparaffinized in xylene and rehydrated through graded decreasing concentrations of alcohol. Antigen retrieval was carried out in citrate buffer pH 6 by heating in a pressure-cooker. The sections were then stained with antibodies specific for the detection of S100 (rabbit polyclonal, DAKO, Milan, Italy) and Ki-67 (Mib-1 Clone, DAKO). Appropriate positive and negative controls were included for each antibody test.

Ki-67 positively stained cells were counted in six different fields of each slide (observed with Olympus BX51 microscope), whereas S-100 quantification was performed on digitally acquired images with Photoshop CS5 program. Results have been expressed in percentage with respect to the controls.

Statistical analysis

Data were expressed as the mean ± SD. Significance between experimental groups was determined by one-way ANOVA followed by the Bonferroni's multiple comparison post test using GraphPad InStat software (San Diego, USA). Values of pÒ0.05 were considered statistically significant.

RESULTS

Preparation and characterization of the inclusion complex of HNE with PACM-ßCD

The chemical structure of the PACM-ßCD conjugate, obtained as previously described [30] is shown in the upper part of Fig. 1A. This conjugate carries a single β-CD moiety at one terminus, characterized by a lipophilic inner cavity and a hydrophilic outer surface, and the PACM chain as an amphiphilic tail. This conjugate, acting as a nanocarrier, is able to solubilize considerable

amounts of poorly soluble drugs and slowly release them, as demonstrated in the case of Acyclovir [30]. At the bottom of Fig 1A, a schematic representation of HNE/PACM-ϐCD is reported. HNE, the guest molecule, is hosted inside the toroidal structure of the ϐCD ring. The host-guest molar ratio is 1:1.

In Fig. 1B the preparation scheme used to prepare HNE/PACM-ϐCD is presented. This conjugate has an average molecular weight in the order of 10^4 Dalton. Thus, their β-CD content is approximately 10% by weight. PAMC-ϐCD was able to encapsulate HNE forming a stable inclusion complex. The HNE/PACM-ϐCD complex gave a clear system after dispersion in water. The HNE loading was about 18 % on a weight to weight basis with an encapsulation efficiency of 83.5 %.

DSC analysis of HNE/PACM-ϐCD confirmed the HNE complexation (data not shown). Moreover, we demonstrated by HPLC determination that the HNE /PACM-ϐCD complex can be stored for 12 months at -20 °C without HNE degradation and after autoclaving procedures (data not shown). The inclusion complex HNE/PACM-ϐCD is stable with a high value of association constant (data not shown). This feature has been also demonstrated by analyzing the *in vitro* release profile of HNE from HNE/PACM-ϐCD in PBS at pH 7.4, to mimic physiological conditions (Fig. 2A). The *in vitro* release profile showed a pseudoï zero order kinetic with no initial burst effect. Under the experimental conditions adopted, about 6 % (w/w) of the drug was released in 2 h, while after 24 h a HNE release of about 30% (w/w) was observed.

Moreover, in order to check the level of protection being offered by the nanocarrier PACM-ϐCD, we measured the ability of HNE to form Michael adducts with His residues of BSA by Western Blot (Fig. 2B). A very strong band of ~60 kDa can be observed only after the incubation of BSA with 10 ε M free HNE, while a faint immunoreaction was observed when BSA was incubated with 10 ε M HNE/PACM-ϐCD. No immunoreaction was observed in control samples (BSA alone or BSA incubated with the empty carrier PACM-ϐCD).

HNE/PACM-ϐCD inhibits cell viability and cell growth in tumor cell lines of several different tissue origins

Figures 3-5 show the amount of viable cells, measured by MTT metabolic assay, after HNE/PACM-ϐCD treatments, at the concentrations indicated, in tumor cell lines of several different tissue origins. In these cell lines the effects on cell viability were compared to those obtained by incubating tumor cell lines with free HNE, at the same concentrations, and with the empty carrier PACM-ϐCD, at dilutions corresponding to that of HNE-loaded inclusion complex.

In all the cell lines tested, 10 ε M HNE/PACM-ϐCD significantly reduced the amount of viable cells, not only in comparison with untreated control cells, but also with respect to cells treated with 10 ε M free HNE.

Human prostate cancer PC-3 cells and human melanoma A375 cells (Fig. 3), human leukemia HL-60 and U937 cells (Fig. 4), were the most sensitive. In these cells, 5 ε M HNE/PACM-ϐCD was still effective in reducing the amount of viable cells, while all the treatments with 1 ε M were uneffective.

In colon carcinoma HT-29 and murine renal carcinoma RenCa cells (Fig. 5), only HNE/PACM-ϐCD 10 ε M treatments were able to reduce the amount of viable cells.

The treatment with the empty PACM-ϐCD did not affect the amount of viable cells in any cell lines tested.

Cell viability was analyzed by trypan blue exclusion test also, in HL-60, PC3 and A375 cell lines, the most sensitive cell lines. All three cell lines were treated with the highest concentration of compounds (10 ε M) and cell viability was analyzed at 24 h - 48 h and 72h (Fig. 6A). In all the three cell lines, 10 ε M HNE/PACM-ϐCD significantly inhibited cell viability at 48 h and 72 h. Moreover, at 72 h this inhibition was significant not only in comparison with untreated control cells, but also with respect to cells treated with 10 ε M free HNE. A modest but significant inhibition of cell viability was observed in PC3 and A375 cell lines at 72 h after 10 ε M free HNE treatment.

Cell growth inhibition was evaluated in HL-60, PC3 and A375 cell lines with the highest concentration of the compounds, by counting the number of non-stained viable cells at the indicated time (Fig. 6B). Results demonstrated that in 10 εM HNE/PACM-βCD treated cells, the growth was more reduced with respect to cells treated with 10 εM free HNE.

HNE/PACM-βCD induces apoptosis in PC3, A375 and HL-60 cell lines

In consideration of the great effect on cell viability and cell proliferation, we decided to investigate a possible pro-apoptotic role of HNE/PACM-βCD by studying the presence of cleaved PARP, a hallmark of the terminal apoptotic cascade (Fig. 7). HL-60, A375 and PC3 cell lines, which previously showed great sensitivity toward HNE, where analyzed. Western blot analysis, performed 24 h after cell treatments, revealed an 85-kDa band, corresponding to the main fragment of cleaved PARP, in all the cell lines, after 10 εM HNE/PACM-βCD treatment. A weak band was detected in A375 and a very faint one in PC3 cells treated with 10 εM free HNE, while apoptosis was not present in untreated control cells, as well as in PACM-βCD treated cells.

HNE/PACM-βCD induces differentiation in the HL-60 cell line

HL-60 cells are a tumor cell line well known for differentiation studies. Moreover in our laboratories we have demonstrated the differentiative effect of 1 εM HNE repeatedly added (10 treatments every 45 min) to HL-60 cell suspension [34]. Thus, these previous results prompted us to investigate a possible differentiative effect of HNE/PACM-βCD in the HL-60 cell line. The results were compared to those obtained by treating cells with the empty carrier PACM-βCD, with 10 εM free HNE (a single treatment, HNE ST 10 εM), with 1 εM free HNE repeatedly added (10 treatments every 45 min, HNE RT 1 εM) and with 1.25% DMSO, a well known inducer of differentiation (Fig. 8).

The differentiation was evaluated by the NBT test and the results are expressed in arbitrary units, placing the value 1 to the untreated control. As shown in Fig. 8, 10 εM HNE/PACM-βCD

treatments induced HL-60 differentiation, similarly as obtained by DMSO and HNE-RT. The single treatment with 10 εM free HNE (HNE ST 10 εM) was not sufficient to induce the differentiation program, since the values are very similar to those obtained in untreated controls. Finally, the empty carrier PACM-ϐCD did not induce HL-60 cell differentiation.

The HNE/PACM-ϐCD inclusion complex protects HNE from the reaction towards proteins contained in the medium with FCS.

In order to establish whether HNE loaded into the PACM-ϐCD inclusion complex is more stable in the culture medium containing FCS with respect to free HNE, we measured its rate of disappearance by HPLC (Fig. 9A). HPLC analysis can detect only reactive and free HNE, not already bound to other molecules, thus it is possible to measure molecules of aldehyde still capable of binding to molecular targets. The concentration of HNE was measured in culture medium containing serum, after the addition of 10 εM HNE/PACM-ϐCD or 10 εM free HNE at 5, 15 and 30 min. At 5 min a non significant difference was already present between the two samples: reactive HNE level was higher in the medium treated with 10 εM HNE/PACM-ϐCD with respect to 10 εM free HNE treated medium (about 95% and 80% of remaining HNE in 10 εM HNE/PACM-ϐCD and 10 εM free HNE treated medium, respectively). After 15 min, HNE loaded in the PACM-ϐCD inclusion complex was almost entirely present in the medium (about 90% of remaining HNE), while free HNE was greatly diminished (about 60% of remaining HNE). At 30 min more than 70% of HNE was still present, if protected by the nanocarrier, while free HNE almost totally disappeared (about 20% of remaining HNE).

PACM-ϐCD nanocarrier preserves HNE reactivity in HL-60 cell suspension

The rate of disappearance of reactive HNE was also measured in a homogeneus cellular suspension of HL-60 cells after 10 εM HNE/PACM-ϐCD addition, in comparison with data obtained by treating HL-60 cells with 10 εM free HNE (Fig. 9B). At 5 min a dramatic decrease in reactive HNE

content was observed in the cell suspension treated with 10 εM free HNE (about 55% of remaining HNE), while in the cell suspension, treated with 10 εM HNE/PACM-ϐCD, HNE there was a slight decrease (about 90% of remaining HNE). At 15 min the reactive HNE level decreased in both conditions, but more consistently in the cell suspension treated with 10 εM free HNE (about 80% and 30% of remaining HNE in 10 εM HNE/PACM-ϐCD and 10 εM free HNE treated cells, respectively). At 30 min a similar diminishing trend was observed; however, although at 30 min the reactive HNE level in cell suspension treated with 10 εM HNE/PACM-ϐCD decreased by half compared to its level at 15 min, its concentration was significantly higher with respect to that measured in the cell suspension treated with 10 εM free HNE (about 40% and 13% of remaining HNE in 10 εM HNE/PACM-ϐCD and 10 εM free HNE treated cells, respectively)

PACM-ϐCD inclusion complex is rapidly internalized within cells.

The penetration of our formulation inside the cells was evaluated in HL-60, A375 and PC3 tumor cell lines. The fluorescent labeled 6-coumarin PACM-ϐCD inclusion complex was added to the cell suspensions and evaluated by confocal laser scanning microscopy at 1, 5 and 45 min in fresh cells (Fig. 10).

In all the cell lines, the 6-coumarin PACM-ϐCD inclusion complex immediately came inside the cells (within 1 min, data not shown). After 5 min cell incubation, the distribution was cytoplasmatic and similar results were obtained at 45 min after the treatment. Fluorescence was not detected in cells not exposed to labeled PACM-ϐCD inclusion complex (data not shown).

Inside cells, HNE loaded in PACM- ϐCD is released from the nanocarrier and reacts with proteins.

In order to investigate the ability of PACM- ϐCD inclusion complex to release HNE inside cells, thus rendering it able to react with intracellular targets, we analyzed the presence of HNE protein adducts in HL-60 cells at 5, 15 and 45 min after treatments with 10 εM HNE/PACM- ϐCD. Results were compared to those obtained by treating HL-60 cells with 10 εM free HNE. HNE-His adducts

were detected by immunofluorescence and representative results are showed in Fig. 11. Five min after 10 εM free HNE addiction, HNE-protein adducts can be located mainly on the surface of the plasma membrane, while in 10 εM HNE/PACM- ϐCD treated cells we observed a weak immunofluorescence signal. After 15 min, both cells treated with 10 εM free HNE and 10 εM HNE/PACM- ϐCD showed HNE-protein adducts. The same feature was observed at 45 min. No traces of HNE-adducts were detected in not-treated control cells (data not shown).

HNE/PACM-ϐCD inhibits melanoma cell growth in a human 3D culture

As previously reported in this paper, HNE/PACM-ϐCD greatly inhibits the A375 human melanoma tumor cell line (Fig. 3). This prompted us to investigate the effect of HNE/PACM-ϐCD on a more complex experimental model, such as the three-dimensional skin reconstruction model of A375 melanoma cells. Culture inserts were incubated in duplicate with serum-free medium containing PBS (Control), 10 εM HNE/PACM-ϐCD, 10 εM free HNE or the empty carrier PACM-ϐCD, at the dilution corresponding to that of the HNE-loaded inclusion complex. The medium was replenished every other day and cell cultures were collected before the treatment (day 0) and on days 3 and 8 from the beginning of the treatments. H&E staining of day 0 cultures (data not shown) revealed keratinocytes in the upper epidermal layer, organized in the basal, spinous, granular and corneum stratum; a second distinct layer of cells was represented by A375 melanoma cells. At this early time point, this layer is only a few cells thick, and these cells are distinguished by their dark nuclear staining. The third distinct layer is represented by fibroblast-contract collagen, the dermal stratum. Over time, in control culture inserts, the metastatic melanocytes proliferate and develop nodules by day 3 (data not shown), larger at day 8 (Fig. 12). In contrast, at day 8, culture treated with 10 εM HNE/PACM-ϐCD had smaller tumor nodules and remain closer to the epidermidis with lower invasion of the dermal structures. Intermediate results were obtained at day 8 with 10 εM free HNE; at this time tumor nodules were smaller than those observed in control specimens, but larger than those observed in 10 εM HNE/PACM-ϐCD treated culture inserts. Finally, conditions similar

to those observed in control culture inserts were obtained in PACM-ϐCD-treated 3D cultures (Fig. 12).

The analysis for the expression of the S100 protein, a marker of melanocytes/melanoma cells, confirmed the presence of melanoma cells in the tissues. Fig. 13 reveals strong expression of S-100 in control culture inserts, as well as in tissue cultures treated with the empty vehicle PACM-ϐCD. In contrast, 10 ε M HNE/PACM-ϐCD significantly inhibited S-100 expression, while with free HNE we observed intermediate results. These observations were quantified and the densitometric results are presented in Fig. 14. To determine whether the decrease of S-100 positive cells might account for the inhibition of melanocyte proliferation, tissue sections were stained with the proliferation marker Ki-67. The Ki-67 staining (Fig. 13) clearly reveals a decrease in the number of proliferative cells after treatment with 10 ε M HNE/PACM-ϐCD, with respect to control or PACM-ϐCD-treated tissues. Intermediate results were obtained, again, with free 10 ε M HNE treatments. A quantitative analysis of the immunohistochemical results of Ki-67 is presented in Fig. 14.

The nanotechnological formulation did not have toxic effects on normal cells, such as fibroblasts and keratinocytes making up the three dimensional tissue.

DISCUSSION

The results presented in this experimental work demonstrate that PACM-ϐCD conjugate was able to complex HNE, improving the water solubility and stability of the lipophilic aldehyde. The *in vitro* release results indicated a very slow release rate for HNE, demonstrating a stable host-guest non-covalent interaction. When HNE is inside the PACM-ϐCD nanocarrier, it is not able to form Michael adducts with proteins, one of the key events in the biological responses to the aldehyde. Moreover, in the medium containg FCS, in presence or in absence of cells, the nanocarrier keeps the reactive groups of HNE in a free form, not bound to other molecules. All these results strongly

suggest that HNE, loaded in the PACM-ϐCD nanocarrier, is more protected from its degradation, catabolization or reaction towards extracellular targets.

As soon as PACM-ϐCD is added to a cellular suspension, the nanocarrier is rapidly internalized into the cells (within 1 min), as demonstrated from results obtained by confocal microscopy. Although it is not possible, for technical reason, to mark with a fluorescent dye, such as 6-coumarin, the PACM-ϐCD carrying HNE, we succeeded in demonstrating the release of HNE inside the cells after 10 ε M HNE/PACM-ϐCD treatment, through the detection of HNE-protein adducts. Indeed, we have previously demonstrated that PACM-ϐCD protects HNE from the reaction with proteins; thus, the presence of HNE-protein adducts inside cells strongly suggests that HNE was released form the nanocarrier a few minutes after uptake. Moreover the time course of adduct formation indicated that there were differences in the rate of adduct formation between samples treated with free HNE and HNE/PACM-ϐCD. As already demonstrated in our laboratories [7], free HNE rapidly enters inside cells, by diffusing through cell membranes, so that it is immediately able to form HNE-protein adducts in particular with plasma membrane and cytosolic proteins. Afterwards HNE-protein adducts are more distributed inside cells, forming adducts after 2 h also in the nuclear compartment [7]. The HNE loaded in the *PACM- ϐCD,* being protected by the nanocarrier, is not immediately able to form HNE-protein adducts in the first minutes. However, progressively, HNE can be released from PACM- ϐCD and by 15 min on it is possible to observe widespread HNE-protein adducts, similar to that obtained in 10 ε M free HNE treated cells.

The enhanced stability of HNE, when residing in the nanocarrier, elicited greater biological effects than free HNE in the tumor cell lines analyzed. Indeed, HNE/PACM-ϐCD was more effective in reducing cell viability and cell growth with respect free HNE, in all the cell lines tested. Moreover, we have demonstrated that 10 ε M HNE/PACM-ϐCD induced apoptosis in HL-60, PC3 and A357 cells at 24 h, while the contribution of apoptosis in affecting cell viability is very small or completely absent in free HNE treated cells. These results are in agreement to those obtained with the trypan blue assay, where an increase of cell death can be observed after 10 ε M HNE/PACM-

ϐCD treatments at 48 h and, more consistently, at 72 h, compatible with a secondary necrosis. A similar observation can be made for PC3 and A375 treated with 10 ε M free HNE, where faint bands of cleaved PARP can be observed at 24 h in both cell lines, paralleling a weak, but significant, increase of stained trypan blue cells at 72 h. Further, in HL-60 cells, we have demonstrated that 10 ε M HNE/PACM-ϐCD induced not only apoptosis but also cellular differentiation, while a single treatment with 10 ε M free HNE did not. We previously demonstrated that differentiation induction occurred when HL-60 cells were maintained for 7.5 h in presence of 1 ε M HNE through the protocol of repeated treatments [34]. Thus, it appears that the activity in the induction of cell differentiation, which has been found to be higher in 10 ε M HNE/PACM-ϐCD than in 10 ε M free HNE treatment, can be related to the increased permanence of the aldehyde in the cell culture.

Considering the overall results on cellular responses, we can suggest that the protection offered by the nanocarrier to the HNE molecule, allows avoidance of nonspecific interactions with extracellular serum protein, the introduction into cells of a greater number of molecules of reactive HNE and the slow-down of HNE catabolism, with a consequent increase of its biological effectiveness.

Advanced melanoma remains one of the most challenging cancers, in consideration of its resistance to chemotherapy and innovative formulation surely constitutes an innovative therapeutical approach [35]. Thus, results obtained on the human melanoma model are very encouraging, demonstrating a greater inhibitory effect of HNE/PACM-ϐCD with respect to free HNE. The use of a complex experimental model, such as the 3D tissue culture permits creation of a greater similarity between the cultured cells and the living organism. Thus, the reconstruction of the tissue architecture constitutes a relevant feature in increasing the predictability of the experimental model [36]. The effects obtained with HNE/PACM-ϐCD on melanoma tissues are of particular interest, also in consideration of the absence of toxic effects on normal tissues, observed in this experimental work. Indeed, the HNE effect seems to be higher in more undifferentiated melanoma cells with respect to

differentiated normal tissues (epidermal keratinocytes and dermal fibroblasts). These results are in agreement with previous works demonstrating the differing ability of HNE to inhibit proliferation of cells with different degree of differentiation [37]. Moreover, other authors have demonstrated that HNE was more effective in affecting cell proliferation of neoplastic cells with respect to the normal phenotype. For instance, it has been demonstrated that human peripheral blood lymphocytes are more resistant to HNE with respect to human lymphocytic leukemia cells [39] and that HNE is able to eradicate human leukemia stem cells, while it is ineffective on normal erythroid or myeloid progenitors [40]. The same feature has been also observed in solid tumors; indeed, it was demonstrated that HNE was more toxic to osteosarcoma cell lines compared to primary cultures of human osteoblasts [41].

It is well established that cancer cells with increased levels of ROS are more vulnerable to damage by further ROS insults induced by exogenous agents [41]. Indeed, many chemotherapeutic agents induce apoptosis through ROS formation [42], as well as through the induction of lipid peroxidation, generating numerous electrophilic aldehydes, such as HNE [43]. Thus, HNE, during conventional anticancer therapies, can be produced on site and contribute to the process of elimination of tumor cells. Although ROS and HNE have been suggested to be involved in the initiation of cancers, so that the increased oxidative stress is considered as an adverse event, recent papers have indicated that the increasing of oxidative stress can be a novel strategy in cancer therapy [44]. These observations further support the possible use of HNE/PACM-ϐCD as an anti-cancer drug *in vivo*.

REFERENCES

[1] Barrera, G.; Pizzimenti, S.; Dianzani, M. U. Lipid peroxidation: control of cell proliferation, cell differentiation and cell death. Mol. Aspects Med. 29:1ï 8; 2008.

[2] Poli, G.; Schaur, R. J.; Siems, W. G.; Leonarduzzi, G. 4-Hydroxynonenal: a membrane lipid oxidation product of medicinal interest. Med. Res. Rev. 28:569ï 631; 2008.

[3] Barrera G. Oxidative stress and lipid peroxidation products in cancer progression and therapy. ISRN Oncol. In press; 2012.

[4] Esterbauer, H.; Schaur, R.J.; Zollner, H. Chemistry and biochemistry of 4-hydroxynonenal, malonaldehyde and related aldehydes. Free Radic. Biol. Med. 11:81-128; 1991.

[5] Pizzimenti, S.; Toaldo, C.; Pettazzoni, P.; Dianzani, M. U.; Barrera, G. The ñTwo-Facedò effects of reactive oxygen species and the lipid peroxidation product 4-Hydroxynonenal in the hallmarks of cancer. Cancers 2: 338ï 363; 2010.

[6] Stagos, D.; Zhou, H.; Ross, D.; Vasiliou, V. 4-HNE inhibits tube formation and up-regulates chondromodulin-I in human endothelial cells. Biochem. Biophys. Res. Commun. 379:654ï 658; 2009.

[7] Gentile, F.; Pizzimenti, S.; Arcaro, A.; Pettazzoni, P.; Minelli, R.; D'Angelo, D.; Mamone, G.; Ferranti, P.; Toaldo, C.; Cetrangolo, G.; Formisano, S.; Dianzani, M.U.; Uchida, K.; Dianzani, C.; Barrera, G. Exposure of HL-60 human leukemic cells to 4-hydroxynonenal promotes the formation of adduct(s) with alpha-enolase devoid of plasminogen binding activity. Biochem. J. 422:285ï 294; 2009.

[8] Barrera, G.; Muraca, R.; Pizzimenti, S.; Serra, A.; Rosso, C.; Saglio, G.; Farace, M. G.; Fazio, V. M.; Dianzani, M. U. Inhibition of c-myc expression induced by 4-hydroxynonenal, a product of lipid peroxidation, in the HL-60 human leukemic cell line. Biochem. Biophys. Res. Commun. 203:553ï 561; 1994.

[9] Barrera, G.; Pizzimenti, S.; Serra, A.; Ferretti, C.; Fazio, V. M.; Saglio, G.; Dianzani, M. U. 4-Hydroxynonenal specifically inhibits c-myb but does not affect c-fos expressions in HL-60 cells. Biochem. Biophys. Res. Commun. 227:589ï 593; 1996.

[10] Pizzimenti, S.; Barrera, G.; Dianzani, M. U.; Brüsselbach, S. Inhibition of D1, D2, and A-cyclin expression in HL-60 cells by the lipid peroxidation product 4-hydroxynonenal. Free Radic. Biol. Med. 26:1578ï 1586; 1999.

[11] Pizzimenti, S.; Ferracin, M.; Sabbioni, S.; Toaldo, C.; Pettazzoni, P.; Dianzani, M.U.; Negrini, M.; Barrera, G. MicroRNA expression changes during human leukemic HL-60 cell differentiation induced by 4-hydroxynonenal, a product of lipid peroxidation. Free Radic. Biol. Med. 46:282ï 288; 2009.

[12] Barrera, G.; Pizzimenti, S.; Laurora, S.; Moroni, E.; Giglioni, B.; Dianzani, M.U. 4-Hydroxynonenal affects pRb/E2F pathway in HL-60 human leukemic cells. Biochem. Biophys. Res. Commun. 295:267ï 275; 2002.

[13] Laurora, S.; Tamagno, E.; Briatore, F.; Bardini, P.; Pizzimenti, S.; Toaldo, C.; Reffo, P.; Costelli, P.; Dianzani, MU.; Danni, O.; Barrera, G. 4-Hydroxynonenal modulation of p53 family gene expression in the SK-N-BE neuroblastoma cell line. Free Radic. Biol. Med. 38:215ï 225; 2005.

[14] Kutuk, O.; Basaga. H. Apoptosis signalling by 4-hydroxynonenal: a role for JNK-c-Jun/AP-1 pathway. Redox Rep. 12:30-4; 2007.

[15] Awasthi, Y.C.; Sharma, R.; Sharma, A.; Yadav, S.; Singhal, S.S.; Chaudhary, P.; Awasthi, S. Self-regulatory role of 4-hydroxynonenal in signaling for stress-induced programmed cell death. Free Radic. Biol. Med. 45:111-118; 2008.

[16] Pizzimenti, S.; Briatore, F.; Laurora, S.; Toaldo, C.; Maggio, M.; De Grandi, M.; Meaglia, L.; Menegatti, E.; Giglioni B.; Dianzani, M. U.; Barrera, G. 4-Hydroxynonenal inhibits telomerase activity and hTERT expression in human leukemic cell lines. Free Radic. Biol. Med. 40:1578ï 1591; 2006.

[17] Pizzimenti, S.; Menegatti, E.; Berardi, D.; Toaldo, C.; Pettazzoni, P.; Minelli, R.; Giglioni, B.; Cerbone, A.; Dianzani, M. U.; Ferretti, C.; Barrera, G. 4-hydroxynonenal, a lipid peroxidation

product of dietary polyunsaturated fatty acids, has anticarcinogenic properties in colon carcinoma cell lines through the inhibition of telomerase activity. J. Nutr. Biochem. 21:818-26; 2010.

[18] Bartel, D. P. MicroRNAs: genomics, biogenesis, mechanism, and function. Cell 116:281ï 297; 2004.

[19] Uchida, K. 4-Hydroxy-2-nonenal: a product and mediator of oxidative stress. Prog. Lipid Res. 42:318ï 343; 2003.

[20] Uchida, K.; Stadtman, E. R. Modification of histidine residues in proteins by reaction with 4-hydroxynonenal. Proc. Natl. Acad. Sci. U. S. A. 89:4544ï 4548; 1992.

[21] Bruenner, B. A.; Jones, A. D.; German, J. B. Direct characterization of protein adducts of the lipid peroxidation product 4-hydroxy-2-nonenal using electrospray mass spectrometry. Chem. Res. Toxicol. 8:552ï 559; 1995.

[22] Zarkovic, N.; Tillian, M. H.; Schaur, J.; Waeg, G.; Jurin, M.; Esterbauer, H. Inhibition of melanoma B16-F10 growth by lipid peroxidation product 4-hydroxynonenal. Cancer Biother. 10:153ï 156; 1995.

[23] Hartley, D. P.; Ruth, J. A.; Petersen, D. R. The hepatocellular metabolism of 4-hydroxynonenal by alcohol dehydrogenase, aldehyde dehydrogenase, and glutathione S-transferas,. Arch. Biochem. Biophys. 316:197-205; 1995.

[24] Vander Jagt, D. L.; Kolb, N. S.; Vander Jagt, T. J.; Chino, J.; Martinez, F. J.; Hunsaker, L. A.; Royer, R. E. Substrate specificity of human aldose reductase: Identification of 4-hydroxynonenal as an endogenous substrate. Biochim. Biophys. Acta 1249:117ï 126; 1995.

[25] Siems, W.; Grune, T. Intracellular metabolism of 4-hydroxynonenal. Mol. Aspects Med. 24:167- 175; 2003.

[26] Balogh, L. M.; Atkins, W. M. Interactions of glutathione transferases with 4-hydroxynonenal. Drug Metab. Rev. 43:165-178; 2011.

[27] Saha, R. N.; Vasanthakumar, S.; Bende, G.; Snehalatha, M. Nanoparticulate drug delivery systems for cancer chemotherapy. Mol. Membr. Biol. 27:215-231; 2010.

[28] Wang, X.; Wang, Y.; Chen, Z. G.; Shin, D. M. Advances of cancer therapy by nanotechnology. Cancer Res. Treat. 41:1-11; 2009.

[29] Zhang, J.; Ma, P. X. Host-guest interactions mediated nano-assemblies using cyclodextrin-containing hydrophilic polymers and their biomedical applications. Nano Today 5:337-350; 2010.

[30] Bencini, M.; Ranucci, E.; Ferruti, P.; Manfredi, A.; Trotta, F.; Cavalli R. Poly (4-Acryloylmorpholine) oligomers carrying a ß-cyclodextrin residue at one terminus. J. Polym. Sci., Part A, Polym. Chem. 46:1607ï 1617; 2008.

[31] Cavalli, R.; Donalisio, M.; Civra, A.; Ferruti, P.; Ranucci, E.; Trotta, F.; Lembo, D. Enhanced antiviral activity of Acyclovir loaded into beta-cyclodextrin-poly(4-acryloylmorpholine) conjugate nanoparticles. J. Control Release 137:116-122; 2009.

[32] Sylvester, P.W. Optimization of the tetrazolium dye (MTT) colorimetric assay for cellular growth and viability. Methods Mol. Biol. 716:157-168; 2011.

[33] Collins SJ. The HL-60 promyelocytic leukemia cell line: proliferation, differentiation, and cellular oncogene expression. Blood 70:1233-1244; 1987.

[34] Barrera, G.; Di Mauro, C.; Muraca, R.; Ferrero, D.; Cavalli, G.; Fazio, V. M.; Paradisi, L.; Dianzani, M. U. Induction of differentiation in human HL-60 cells by 4-hydroxynonenal, a product of lipid peroxidation. Exp. Cell Res. 197:148-152; 1991.

[35] Bei, D.; Meng, J.; Youan, B.B. Engineering nanomedicines for improved melanoma therapy: progress and promises. Nanomedicine (Lond). 5:1385-1399; 2010.

[36] Baker, B. M.; Chen, C. S. Deconstructing the third dimension: how 3D culture microenvironments alter cellular cues. J. Cell Sci. 125:3015-3024; 2012.

[37] Schneider, L.; Giordano, S.; Zelickson, B. R. S.; Johnson, M. A.; Benavides, G.; Ouyang, X.; Fineberg, N.; Darley-Usmar, V. M.; Zhang J. Differentiation of SH-SY5Y cells to a neuronal

phenotype changes cellular bioenergetics and the response to oxidative stress. Free Radic. Biol. Med. 51:2007ï 2017; 2011.

[38] Semlitsch, T.; Tillian, H. M.; Zarkovic, N.; Borovic, S.; Purtscher, M.; Hohenwarter, O.; Schaur, R. J. Differential influence of the lipid peroxidation product 4-hydroxynonenal on the growth of human lymphatic leukaemia cells and human periopherial blood lymphocytes. Anticancer Res. 22:1689-1697; 2002.

[39] Hassane, D. C.; Guzman, M. L.; Corbett, C.; Li, X.; Abboud, R.; Young, F.; Liesveld, J. L.; Carroll, M.; Jordan, C. T. Discovery of agents that eradicate leukemia stem cells using an in silico screen of public gene expression data. Blood 111:5654-5662; 2008.

[40] Borovic, S.; Cipak, A.; Meinitzer, A.; Kejla, Z.; Perovic, D.; Waeg, G.; Zarkovic, N. Differential sensitivity to 4-hydroxynonenal for normal and malignant mesenchymal cells. Redox Rep. 12:50-54; 2007.

[41] Wu W. S. The signaling mechanism of ROS in tumor progression. Cancer Metastasis Rev. 25:695ï 705; 2006.

[42] Schumacker, P. T. Reactive oxygen species in cancer cells: live by the sword, die by the sword. Cancer Cell. 10:175ï 176; 2006.

[43] Conklin, K. A. Chemotherapy-associated oxidative stress: impact on chemotherapeutic effectiveness. Integr. Cancer Ther. 3:294-300; 2004.

[44] Trachootham, D.; Alexandre, J.; Huang, P. Targeting cancer cells by ROS-mediated mechanisms: a radical therapeutic approach? Nat. Rev. Drug Discov. 8:579-591; 2009.

ACKNOWLEDGEMENTS

This work was supported by University of Turin (ex 60%, to S.P.) and by Progetti di Ricerca di Ateneo ï Anno 2011 (to G.B.). We thank Dr. Paola Gamba and Dr. Gabriella Testa for assistance on confocal imaging.

FIGURE LEGENDS

Figure 1 (A) Up: chemical structure of ß-cyclodextrin-poly(4-acryloylmorpholine) conjugate; down: schematic representation of HNE/PACM-ßCD (B) Stepwise schematic representation of the HNE/PACM-ßCD conjugate preparation.

Figure 2 (A) *In vitro* release profiles of HNE from PACM-ßCD complex in phosphate buffer at pH 7.4. (B) Western blot of anti HNE-His Michael adduct antibody from addition of different HNE formulations to a BSA solution. Lanes: (1) untreated BSA, (2) PACM-ßCD (3) 10 εM HNE, (4) 10 εM HNE/PACM-ßCD,. Ponceau red staining was used to confirm equal protein loading.

Figure 3 Cell viability evaluated by MTT assay in PC3 and A375 cells. Cell lines were untreated (control) or treated with 10, 5, 1 εM free HNE or HNE/PACM-ßCD or PACM-ßCD at the time indicated. ■ control; ○ PACM-ßCD; ● HNE/PACM-ßCD; ▲ HNE. Results are presented as mean ± SD for four independent experiments. *pÒ0.05, **pÒ0.01 vs. control; ÀpÒ0.05, ÀÀpÒ0.01 vs. PACM-ßCD.

Figure 4 Cell viability evaluated by MTT assay in HL-60 and U937 cells. Cell lines were untreated (control) or treated with 10, 5, 1 εM free HNE or HNE/PACM-ßCD or PACM-ßCD at the time indicated. ■ control; ○ PACM-ßCD; ● HNE/PACM-ßCD; ▲ HNE. Results are presented as mean ± SD for four independent experiments. *pÒ0.05, **pÒ0.01 vs. control; ÀpÒ0.05 vs. PACM-ßCD.

Figure 5 Cell viability evaluated by MTT assay in HT-29 and RenCa cells. Cell lines were untreated (control) or treated with 10, 5, 1 εM free HNE or HNE/PACM-ßCD or PACM-ßCD at the time indicated. ■ control; ○ PACM-ßCD; ● HNE/PACM-ßCD; ▲ HNE. Results are presented as

mean ± SD for four independent experiments. *pÒ0.05, **pÒ0.01 vs. control; ÀpÒ0.05, ÀÀpÒ0.01 vs. PACM-ßCD.

Figure 6 (A) Cell viability evaluated by trypan blue exclusion test in HL-60, PC3 and A375 cells. Cell lines were untreated (control, C) or treated with 10 µM HNE/PACM-ßCD, PACM-ßCD or 10 µM free HNE at the time indicated. Results are expressed in percentage, as mean ± SD for four independent experiments. *pÒ0.05, **pÒ0.01 vs. control; ÀpÒ0.05, ÀÀpÒ0.01 vs. PACM-ßCD. (B) Number of viable cells. Cell lines were untreated (control, C) or treated with 10 µM HNE/PACM-ßCD, PACM-ßCD or 10 µM free HNE at the time indicated. Results are expressed as number of viable cells x 10^{-3} / ml for HL-60 cells and as number of viable cells for PC3 and A375. The mean ± SD for four independent experiments was calculated. *pÒ0.05, **pÒ0.01 vs. control; ÀpÒ0.05, ÀÀpÒ0.01 vs. PACM-ßCD.

Figure 7 Apoptosis induction in HL-60, PC3 and A375 cells. Western blot analysis of cleaved PARP in HL-60, PC3 and A375 cells in untreated control cells (lane A), treated with 10 µM HNE/PACM-ßCD (lane B), or PACM-ßCD (lane C), or 10 µM free HNE (lane D) at 24 h. The same blot was hybridized with anti-ß-actin as loading control.

Figure 8 Differentiation induction on HL-60 cells. Cells were untreated (control, C) or treated with 10 µM HNE/ PACM-ßCD, or with the empty carrier PACM-ßCD, or with 1 µM HNE repeatedly added (10 treatments every 45 min, HNE RT 1 µM), or with 10 µM free HNE (a single treatment, HNE ST 10 µM), or with 1.25% DMSO (DMSO) for 72 h or 96 h. Cell differentiation was determined by NBT test. Results are presented as mean ± SD for three independent experiments. **pÒ0.01 vs. control; ÀÀpÒ0.01 vs. PACM-ßCD.

Figure 9 (A) HNE disappearance in RPMI medium with 10% FCS. 10 ε M HNE/ PACM-ϐCD or 10 ε M free HNE were added to the complete medium. After 5, 15, 30 min, aliquots of medium were analyzed by HPLC. **pÒ0.01 vs. HNE. (B) HNE disappearance in HL-60 cell suspension. 10 ε M HNE/ PACM-ϐCD or 10 ε M free HNE were added to the cell culture. After 5, 15, 30 min, aliquots of medium were analyzed by HPLC. *pÒ0.05 vs. HNE; **pÒ0.01 vs. HNE.

Figure 10 Cell uptake of fluorescent PACM-ϐCD. HL-60, PC3 and A375 cells were incubated with the compound for the indicated times and then analyzed by confocal laser scanning microscopy without fixation. Images were obtained by using plan neofluar lens 20×/0.5 and 40x/0.75 (zoom 2X) in the insets (see Material and Methods section).

Figure 11 Detection of HNE-His adducts by immunofluorescence. HL-60 cells were incubated with 10 ε M free HNE or 10 ε M HNE/PACM-ϐCD. After 5, 15 and 45 min cells were harvested, exposed to the anti-HNE-His antibody and HNE-protein adducts were detected by using a secondary FITC-conjugated antibody. Images were obtained by using plan neofluar lens 40x/0.75.

Figure 12 HNE/PACM-ϐCD effect on A375 melanoma invasion in a 3D tissue model. Culture inserts were incubated in duplicate with serum-free medium containing 10 ε M HNE/PACM-ϐCD (HNE/PACM-ϐCD), free 10 ε M HNE (HNE), PACM-ϐCD, at dilution corresponding to that of HNE-loaded inclusion complex, or PBS for control (Control). Inserts were supplemented with fresh medium containing the corresponding formulations every other day. Representative sections from each treatment, stained with H&E, at day 8 is shown. The top bright red layer represents the epidermis; the next layer of cells with dark blue nuclei represents the melanocyte layer; and the bottom largely unstained area represents the fibroblast-contracted collagen dermal substrate. Serial sections were observed using a 10x/1.30 NA objective lens.

Figure 13 HNE/PACM-ɓCD inhibits proliferation of A375 melanoma cells in a 3D tissue model. Culture inserts were incubated in duplicate with serum-free medium containing 10 ε M HNE/PACM-ɓCD (HNE/PACM-ɓCD), free 10 ε M HNE (HNE), PACM-ɓCD, at dilution corresponding to that of HNE-loaded inclusion complex, or PBS for control (Control). Sections were examined for S100 and Ki-67 expression, by immunohistochemistry. Representative sections from each treatment at day 8 is shown. Serial sections were observed using a 10x/1.30 NA objective lens.

Figure 14 Quantitative analysis of the immunohistochemical results (see fig. 12) depicting the differences in the expression of S100, Ki-67, in 3D tissue cultures treated with 10 ε M HNE/PACM-ɓCD (HNE/PACM-ɓCD), free 10 ε M HNE (HNE), PACM-ɓCD, at dilution corresponding to that of HNE-loaded inclusion complex, or PBS for control (Control). Results are expressed in percentage with respect to control. **pÒ0.01 vs. control.

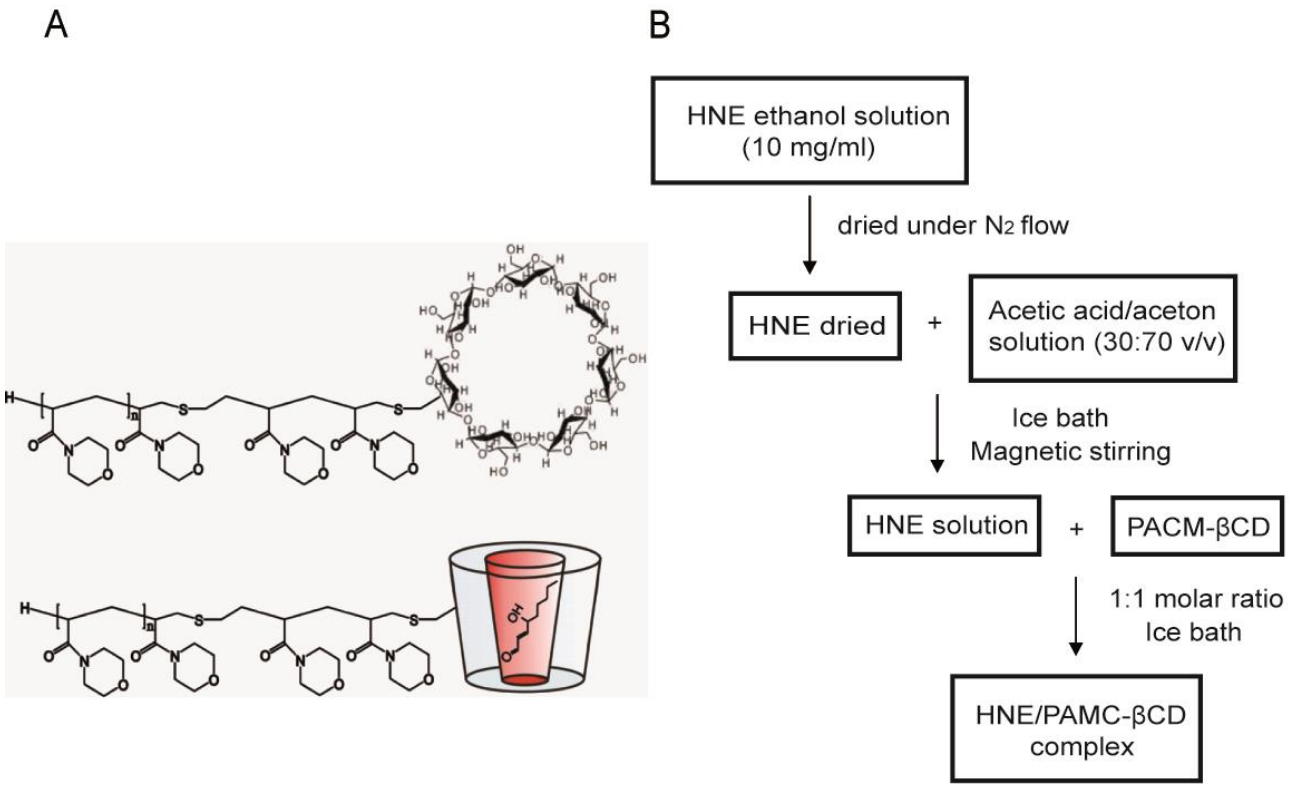
A
B
HNE ethanol solution
(10 mg/ml)
dried under N2 flow
HNE dried
+
Acetic acid/aceton
solution (30:70 v/v)
Ice bath
Magnetic stirring
HNE solution
+
PACM-βCD
1:1 molar ratio
Ice bath
HNE/PAMC-βCD
complex

FIG 1

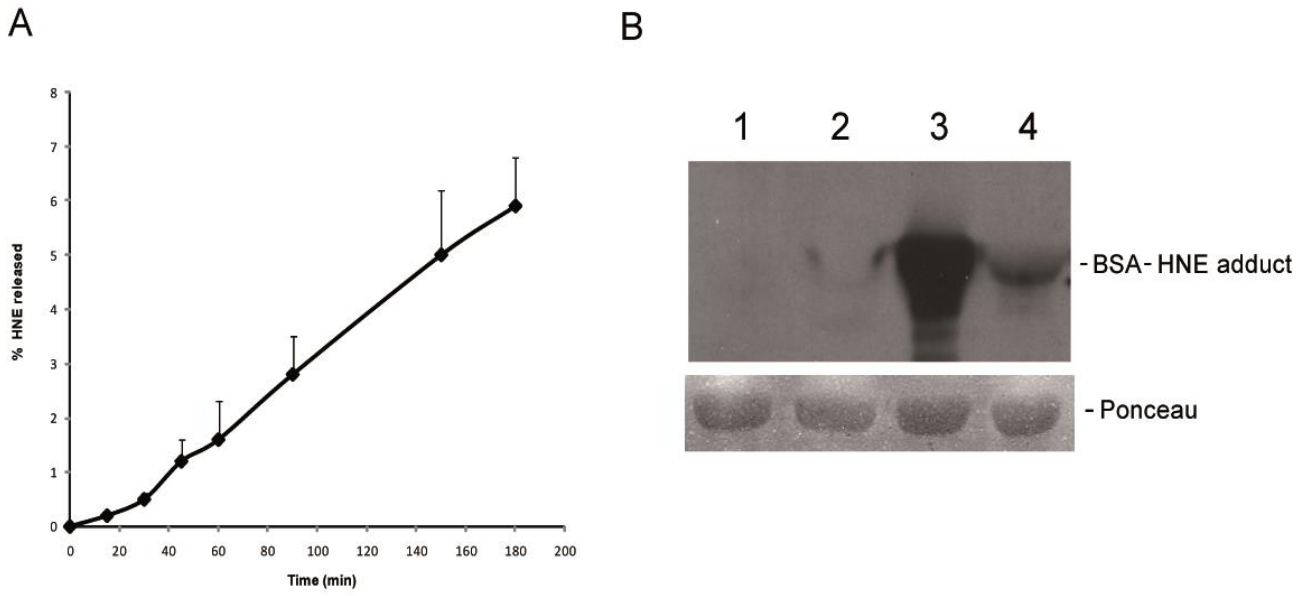
A
B
% HNE released
Time (min)
0
20
40
60
80
100
120
140
160
180
200
1
2
3
4
- BSA- HNE adduct
- Ponceau

fig2

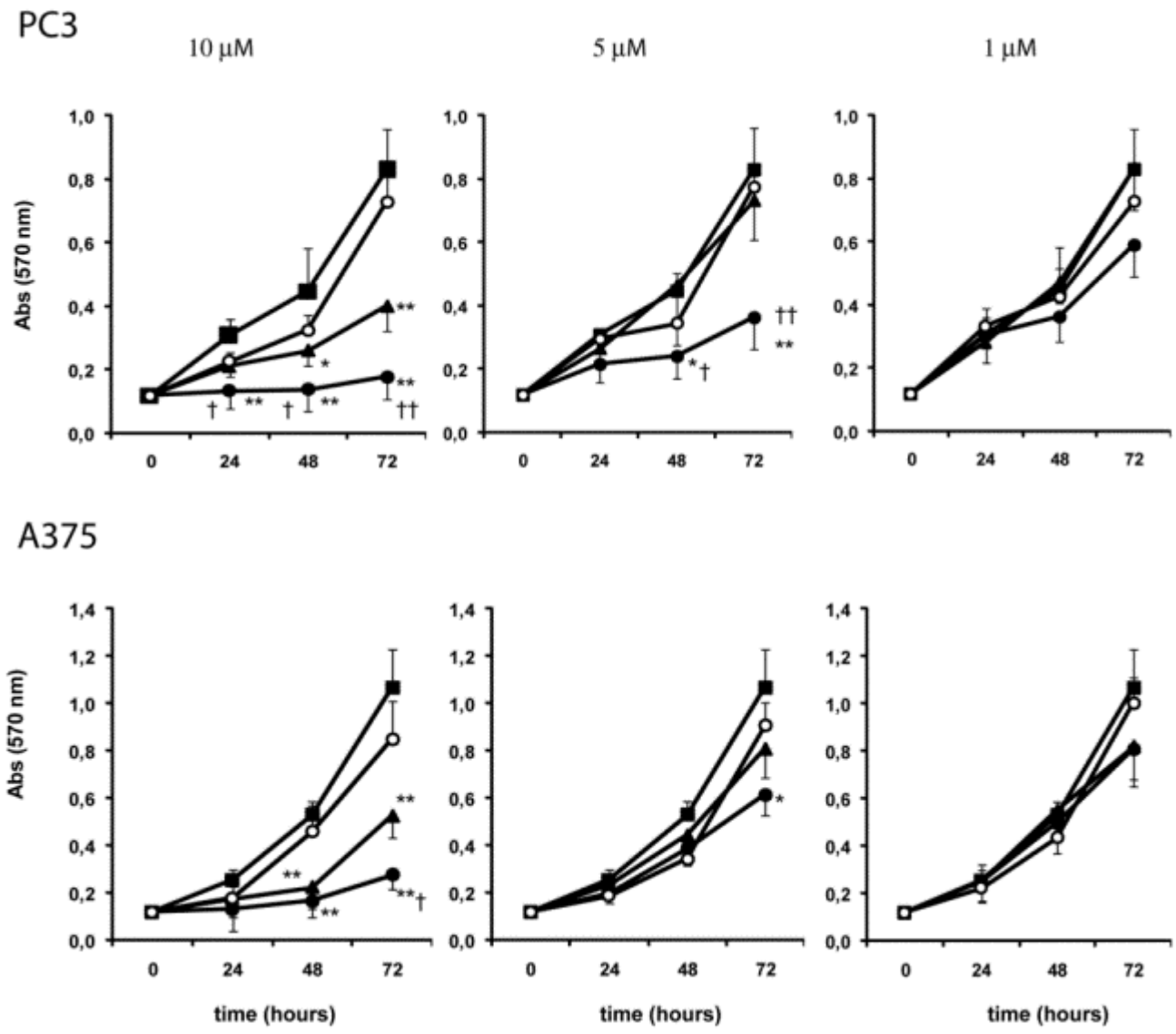

fig3

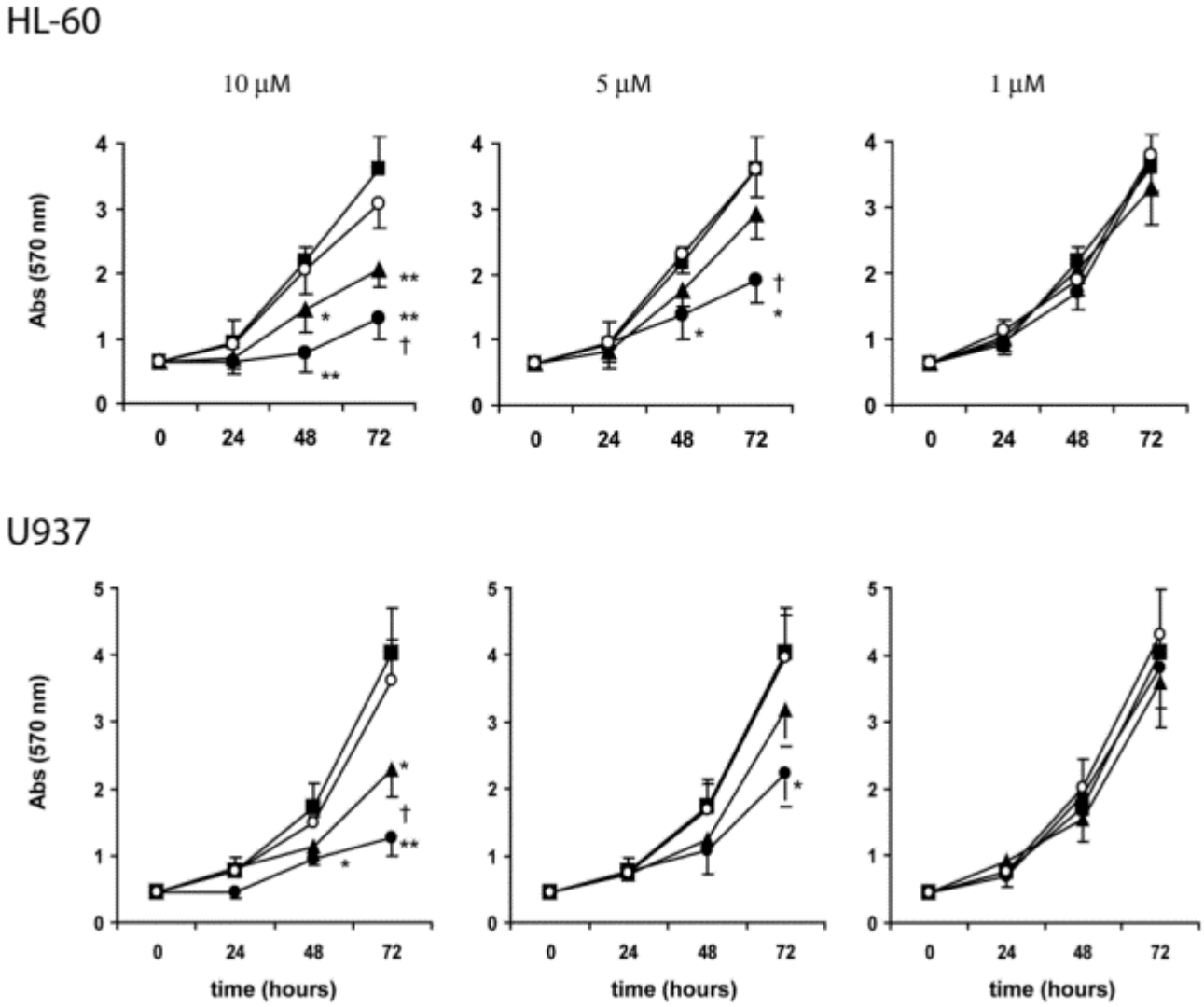

fig4

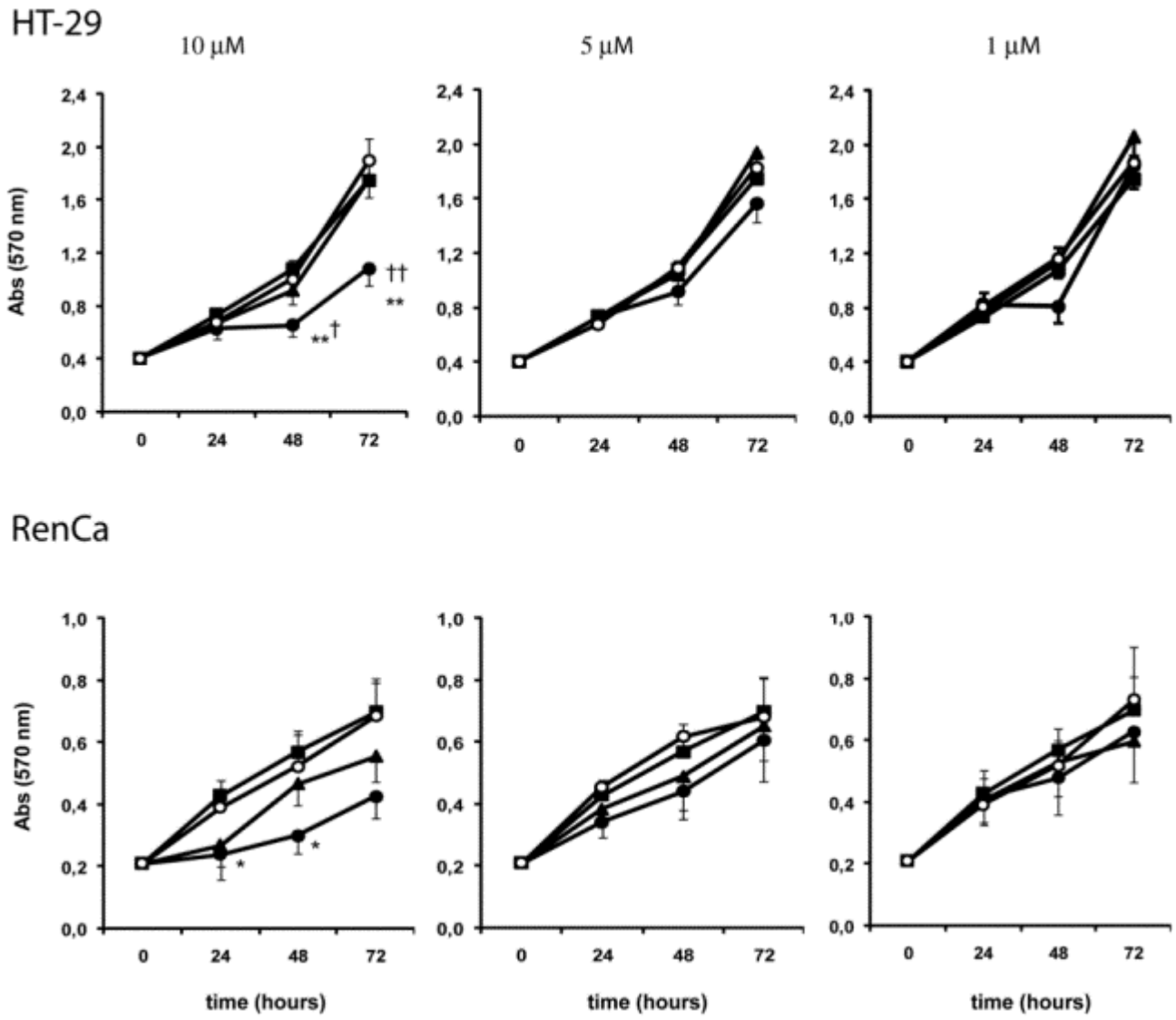
HT-29
10 µM
5 µM
1 µM
Abs (570 nm)
2,4
2,0
1,6
1,2
0,8
0,4
0,0
0
24
48
72
††
**
**†
RenCa
1,0
0,8
0,6
0,4
0,2
0,0
*
*
time (hours)

fig5

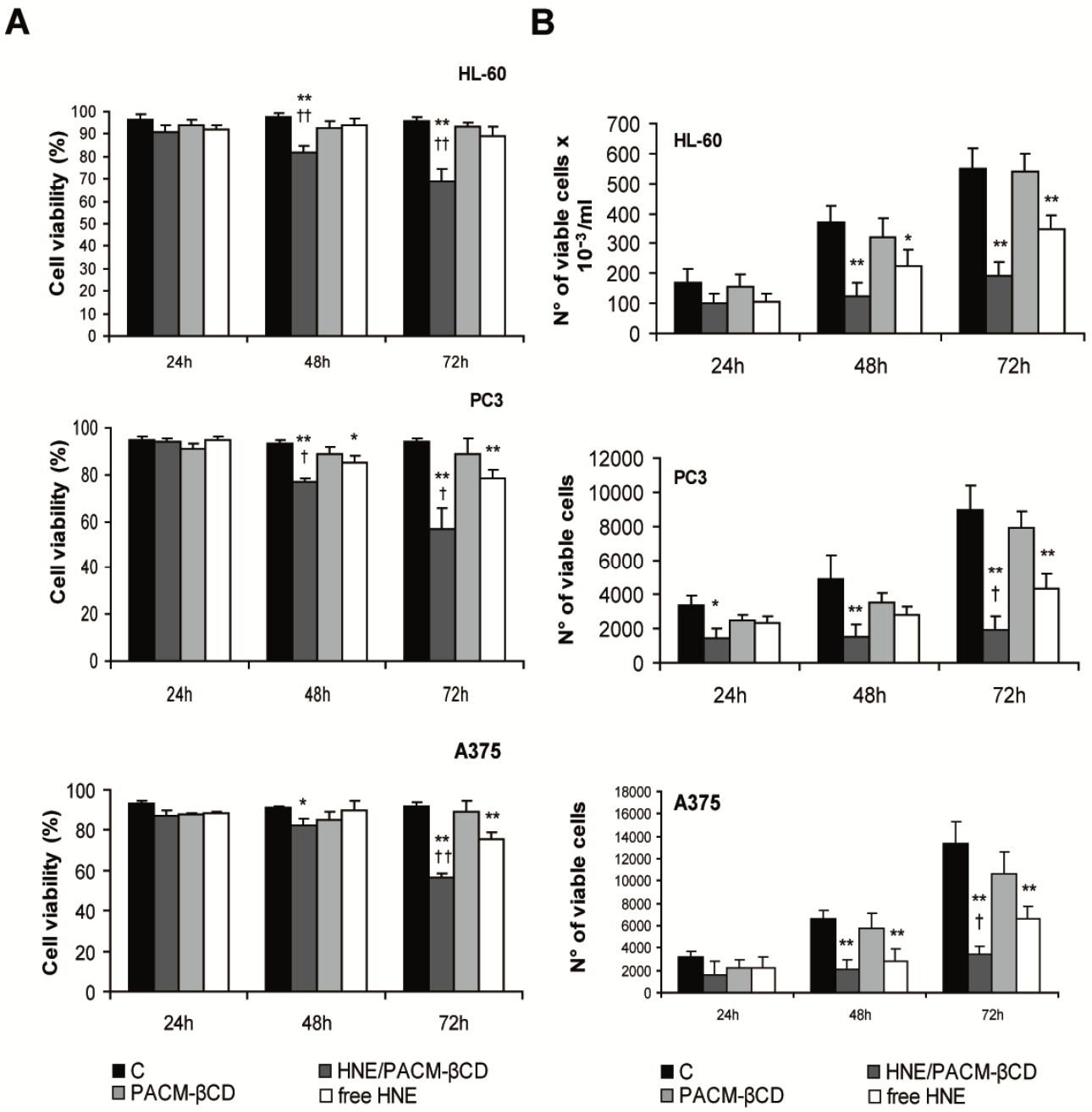
A
B
HL-60
Cell viability (%)
N° of viable cells x 10⁻³/ml
PC3
N° of viable cells
A375
24h
48h
72h
C
PACM-βCD
HNE/PACM-βCD
free HNE

fig6

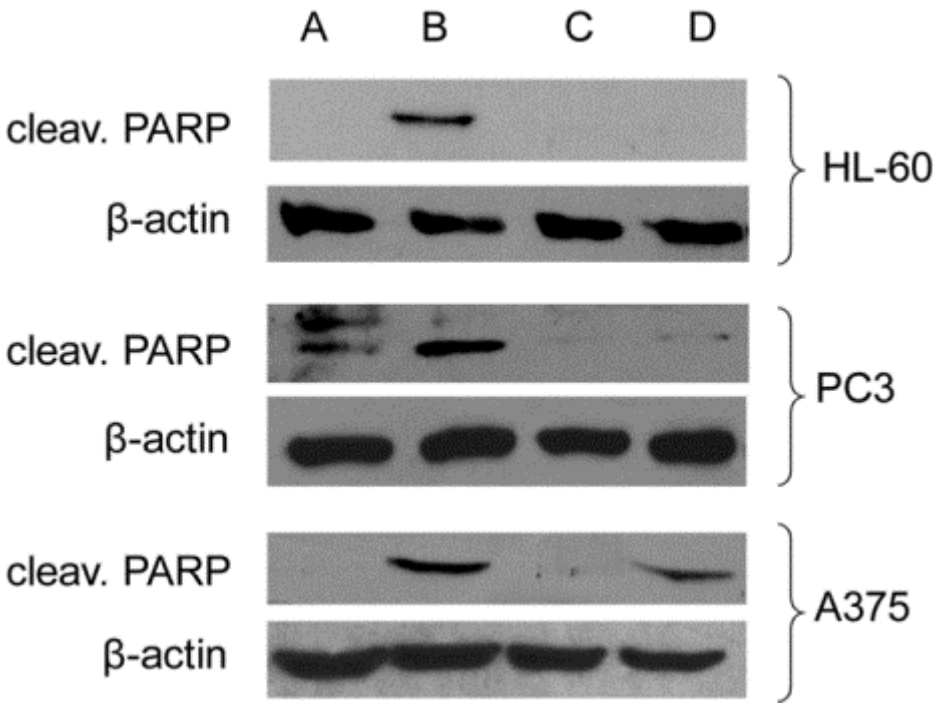
A
B
C
D
cleav. PARP
β-actin
HL-60
cleav. PARP
β-actin
PC3
cleav. PARP
β-actin
A375

fig7

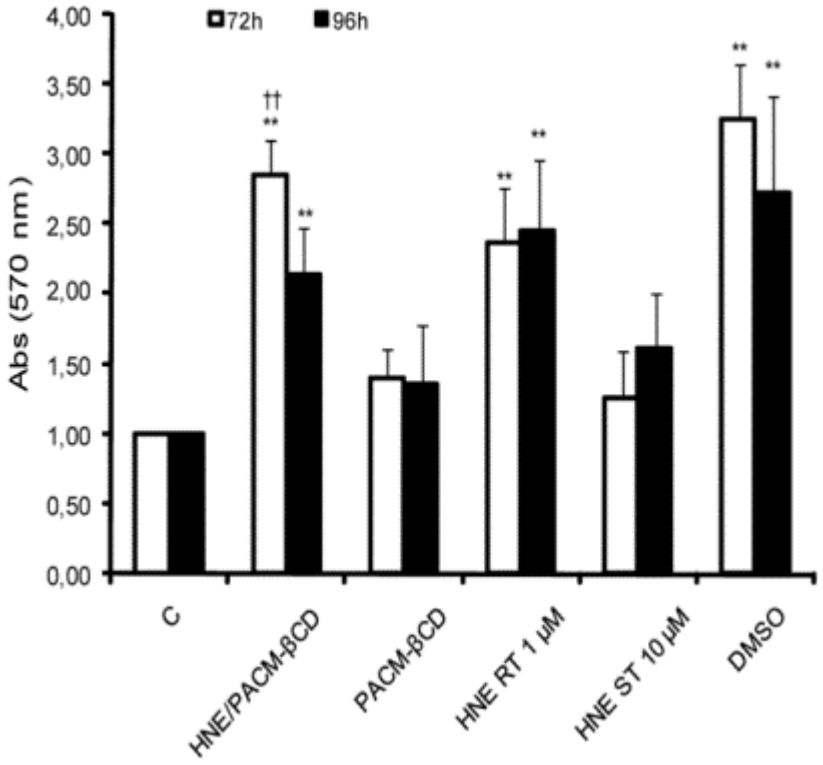
72h
96h
Abs (570 nm)
4,00
3,50
3,00
2,50
2,00
1,50
1,00
0,50
0,00
††
**
C
HNE/PACM-βCD
PACM-βCD
HNE RT 1 µM
HNE ST 10 µM
DMSO

fig8

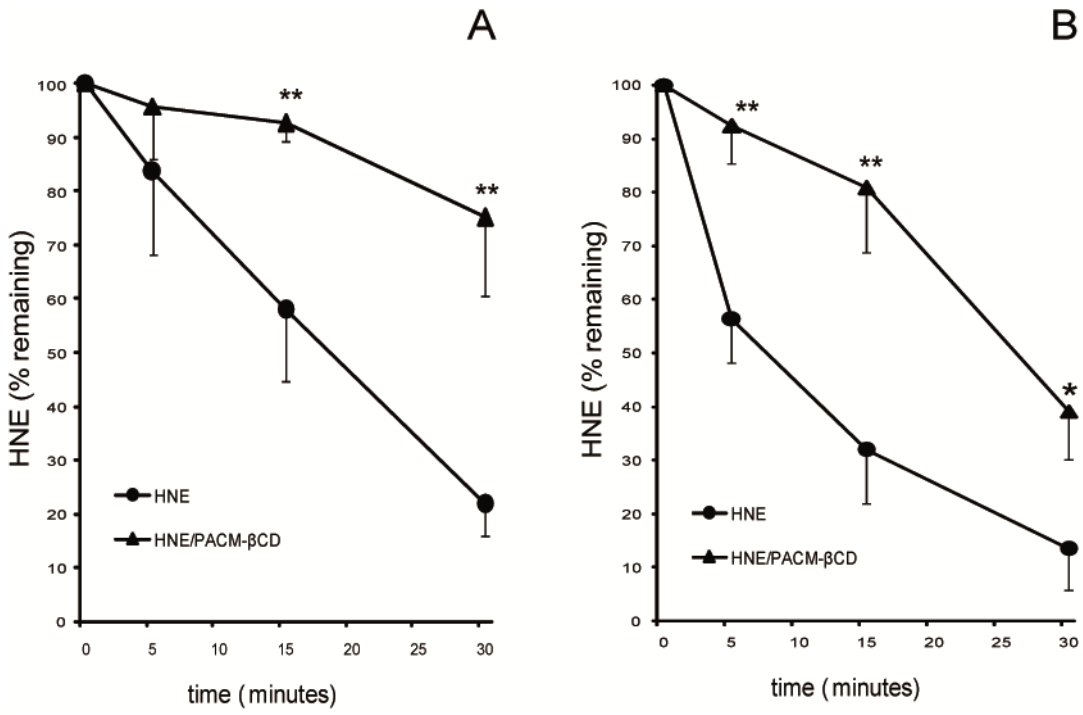

fig9

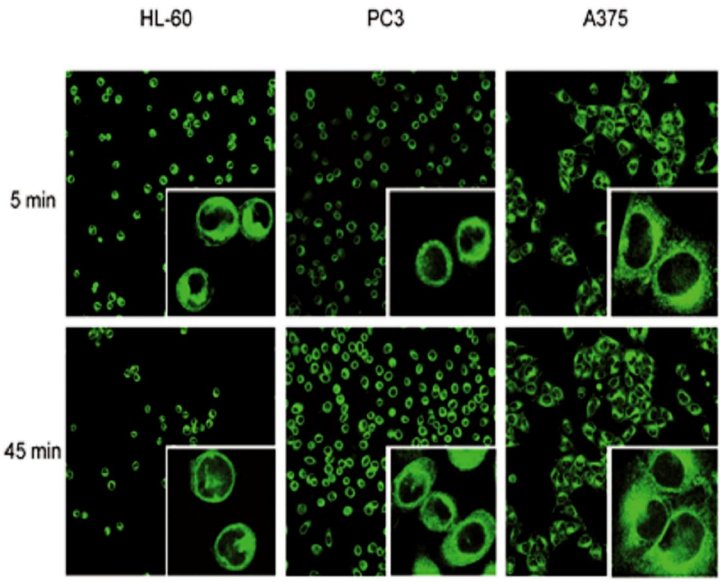

fig10

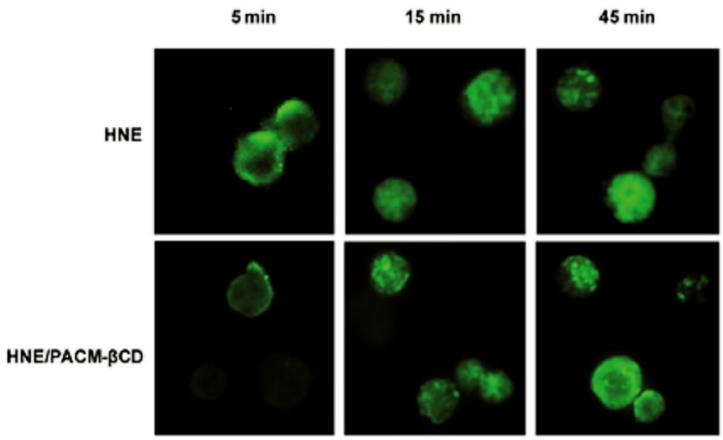

fig11

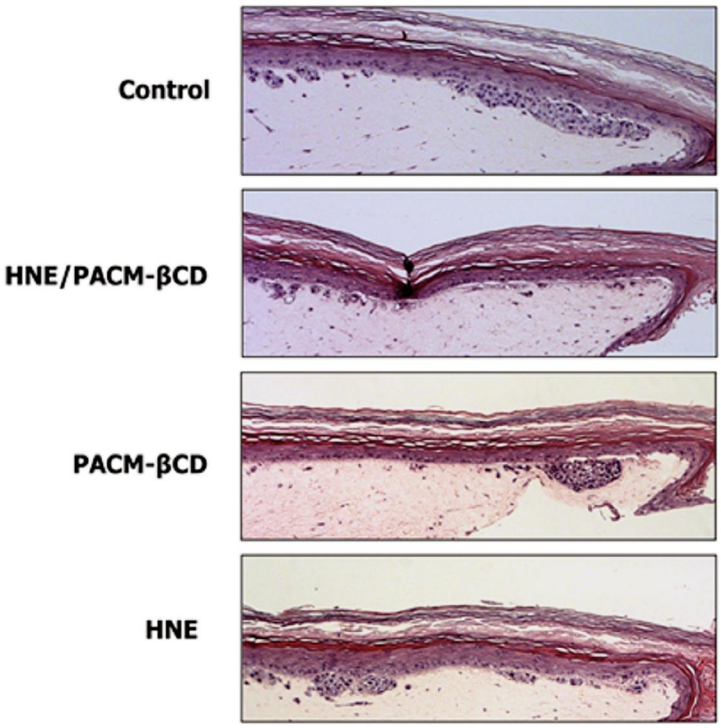

fig12

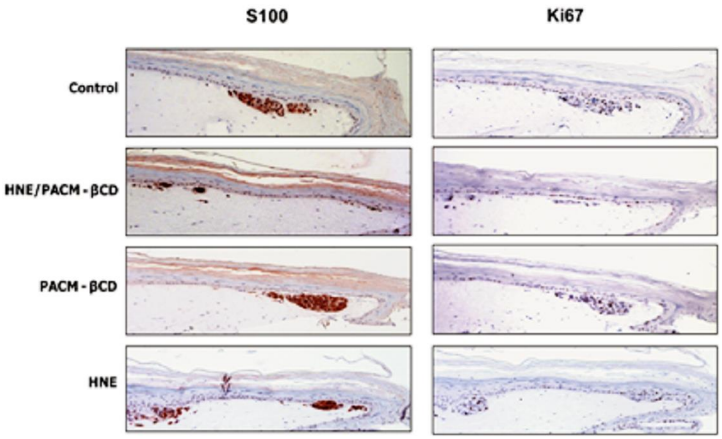

fig13

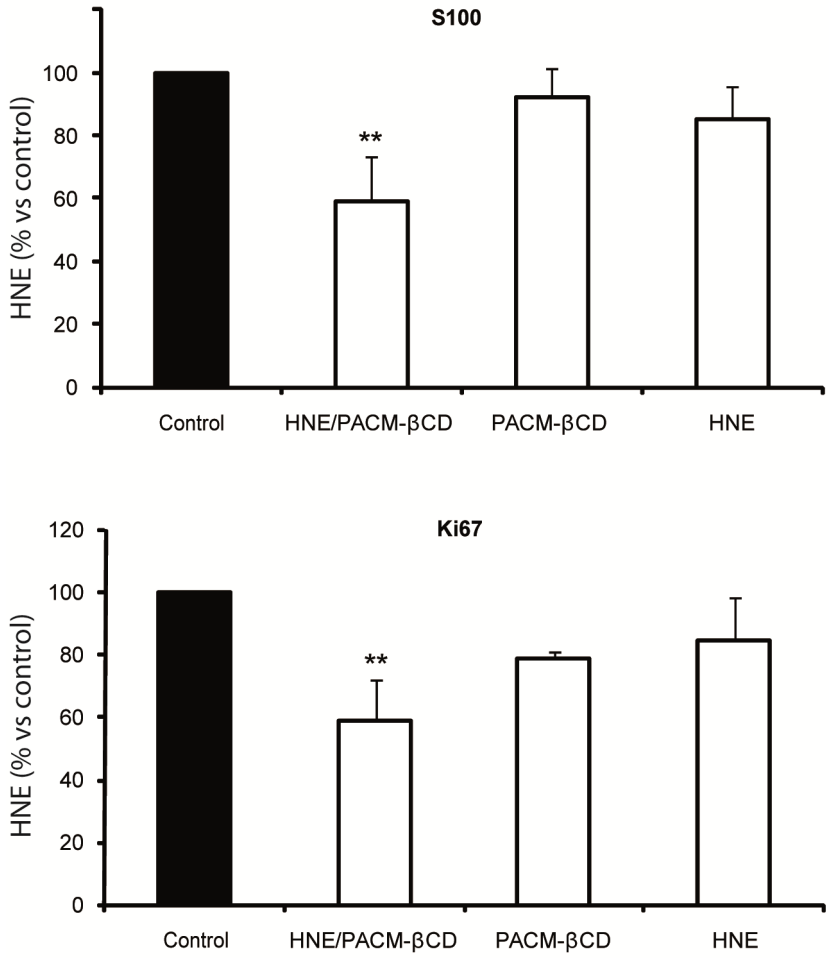
S100
HNE (% vs control)
100
80
60
40
20
0
**
Control
HNE/PACM-βCD
PACM-βCD
HNE
Ki67
HNE (% vs control)
120
100
80
60
40
20
0
**
Control
HNE/PACM-βCD
PACM-βCD
HNE

fig14